La variation séculaire en Amérique Centrale durant la période Maya Classique

First archeointensity determinations on Maya incense burners from Palenque temples, Mexico : New data to constrain the Mesoamerica secular variation curve

G. Fanjat[1], P. Camps[1], L.M. Alva Valdivia[2], M. Sougrati[3], M. Cuevas-Garcia[4] and M. Perrin[5]

[1]Géosciences Montpellier, CNRS and Université Montpellier 2, 34095 Montpellier, France.

[2]Laboratorio de Paleomagnetismo, Instituto de Geofísica, Universidad Nacional Autonoma de Mexico, México D.F., México

[3]Institut Charles Gerhardt, Laboratoire des Agrégats, Interfaces et Matériaux pour l'Energie, 34095 Montpellier, France

[4]Instituto Nacional de Antropologia e Historia, México D.F., México

[5]CEREGE, Europôle Méditerranéen de l'Arbois, Aix en Provence, France

Sumitted to Earth and Planetary Science Letters

Abstract

We present archeointensity data carried out on pieces of incense burners from the ancient Maya city of Palenque, Chiapas, Mexico, covering the Mesoamerican Classic period from 400 to 820 A.D. We worked on pieces from 24 incense burners that were excavated in the Temple of the Cross (13 pieces), Temple of the Foliated Cross (7 pieces), Temple of the Sun (3 pieces) and Temple of the Group XVI (1 piece). The sampling encompasses 5 ceramic phases : Motiepa (400-500 A.D.), Cascadas (500-620 A.D.), Otulum (620-700 A.D.), Murcielagos (700-750 A.D.), and Balunté (750-820 A.D.). Incense burners were used for religious rituals in order to worship the gods who are represented on the pedestal, by burning vegetable resins and probably human blood deposited in the braziers placed above. Iconographic, morphological and stylistic analyses, depending on their provenance and manufacturing technology, allowed to build a reference framework for a temporal classification. All the samples come from incense burners for which the ceramic phase is undoubtedly identified. Archeointensity measurements were performed with the Thellier-Thellier method on pre-selected samples by means of their magnetic properties. We obtained archeointensities of very good technical quality from 19 pieces over the 24, allowing the determination of a precise mean value for each ceramic phase ;

Motiepa : 29.1 ± 0.9 μT, Cascadas : 32.9 ± 1.2 μT, Otulum : 30.5 ± 1.1 μT, Murcielagos : 30.5 ± 0.6 μT and Balunté : 31.7 ± 0.7 μT. The firing temperatures of the ceramics were estimated with Mössbauer spectroscopy between 850 and 1000°C. These values ensure that a full TRM was acquired during the original heating. Our results suggest a relative stability of the field intensity during more than 400 years in Mesoamerica and help to confirm the different ceramic phases. In addition, they clearly argue in favor of a subdivision of the Motiepa phase into an early Motiepa phase (400-500 A.D.) and a Cascadas phase (500-620 A.D.). The abundance of archeological material in Mesoamerica contrasts with the small amount of archeomagnetic data available that are, in addition, of uneven quality. Thus it is especially difficult to establish a trend of intensity variations in Mesoamerica, even using the global databases and secular variation predictions from global models. In this context, our high technical quality data represent a strong constrain for the Mesoamerican secular variation curve during the first millennium A.D. The corresponding Virtual Axial Dipole Moments (VADM) are smaller than the ones predicted by the global geomagnetic models, suggesting the need for additional data to develop a regional model and a reference curve for the Mesoamerica.

Key words : Archeointensity - Palenque - Incense Burner - Secular Variation

2.4.1 Introduction

Records of the ancient geomagnetic field intensity over geological time (paleointensity) and pre-historical and historical time (archeointensity) are unique observations of the temporal evolution of the energy involve in the dynamo processes occurring in the Earth's liquid outer core. Archeomagnetic measurements represent a significant part of the data over the last ten millennia, before the historical records from sailors and the beginning of the continuous direct data acquisition in magnetic observatories and from satellites. Indeed, archeological artifacts made from baked clays such as pottery, kilns, bricks or any other burnt clay structures, supply reliable measurements as they usually carry a strong and stable thermo-remanent magnetization (TRM) acquired during their last firing. Archeomagnetic studies of such pre-historical and historical remains could provide a long and accurate record over the last ten millennia of the geomagnetic field and its secular variation (e.g. compilations of Genevey et al. (2008) and Donadini et al. (2009)). Global geomagnetic models have been built to millennial time scales using such data compilations. The reference global models CALSxk (Continuous model of Archeomagnetic and Lake Sediment data over the x last millennia) and ARCH3k (relying on a selective compilation of only archeomagnetic data), are defined over a time interval from 3 to 10 kyrs (Korte and Constable, 2005, 2011; Donadini et al., 2010; Korte et al., 2011). These models represent a double interest (Gallet et al., 2009). The first concerns the geophysical research. They allow an examination of several questions as varied as the

role of the geomagnetic field on the cosmogenic isotopes production rate (Lifton et al., 2008) or the possible transfer of energy from the geomagnetic dipole to the non-dipole terms (Camps and Prévot, 1996). The second concerns the archeology. Well-established data sets from different regions of the world are necessary to develop dating methods by comparing the geomagnetic field elements (intensity and/or direction) as recorded by an archeological artifact against a master curve of the secular variation of the geomagnetic field (e.g. Lanos et al. (2005); Gallet et al. (2009)). The precision of archeomagnetic datings depends directly on the accuracy of the calibration curves. However, a common deficiency in all of these models is a large spatial bias arising from the fact that most of the data comes from the northern hemisphere, essentially from Europe, linked to a lack of reliable intensity and directional data from the southern hemisphere. Indeed, numerous regional studies have provided high quality archeomagnetic data in several parts of Europe (e.g. compilations of Gallet et al. (2002); Kovacheva et al. (2009); Tema et al. (2010); Tema and Kondopoulou (2011)), because the cultural heritage is very important and numerous investigations have been carried out. These compilations have been used to build regional master curves that allow a precise dating of various archeological artifacts (Kovacheva et al., 2004; Gallet et al., 2009; Aidona and Kondopoulou, 2012).

Surprisingly enough, the secular variation curve of the geomagnetic field in Mesoamerica is rather poorly defined despite of the important amount of archeological sites and the impressive cultural heritage. Data are sparse and are of uneven quality. As a consequence, archeomagnetic dating in Mesoamerica is still a hard task to manage (López-Téllez et al., 2008). Indeed, after the pioneering studies of Nagata et al. (1965) and Bucha et al. (1970), very few studies were performed until recently on archeological artifacts (Ceja et al., 2009; Morales et al., 2009; Alva-Valdivia et al., 2010; Pineda-Durán et al., 2010, 2011) and on historical lava flows (Gonzalez et al., 1997; Morales et al., 2001; Conte-Fasano et al., 2006). The present study is part of this recent effort. We carried out an archeointensity study over 24 incense burners excavated in the Maya city of Palenque (Mexico). Our sampling covers a large part of the Classic period (400-820 A.D.). In the first part of this paper, we describe the archeological context and the samples. Then, we analyze the magnetic mineralogy and the firing conditions of the incense burners during their manufacture. Next, the archeointensty experiments and results are presented. Finally, we discuss the reliability of these results, and a comparison with an appropriate data selection in the Mesoamerican region and global models is attempted.

2.4.2 Archeological context and ceramic ages

The ceramics studied in this paper are pieces of incense burners excavated at the archeological site of Palenque, Chiapas, Mexico, (Fig. **??**), one of the most important Classic Maya cities. Incense burners were one of the main components of the religious

ceremonials in Mesoamerica and were composed of two parts : a hollow clay pedestal surmounted by a brazier. Rice (1999) distinguished two groups of censers, with effigy and without effigy. The effigy censers are characterized by the representation of divinities on the pedestal (Fig. 2.18).

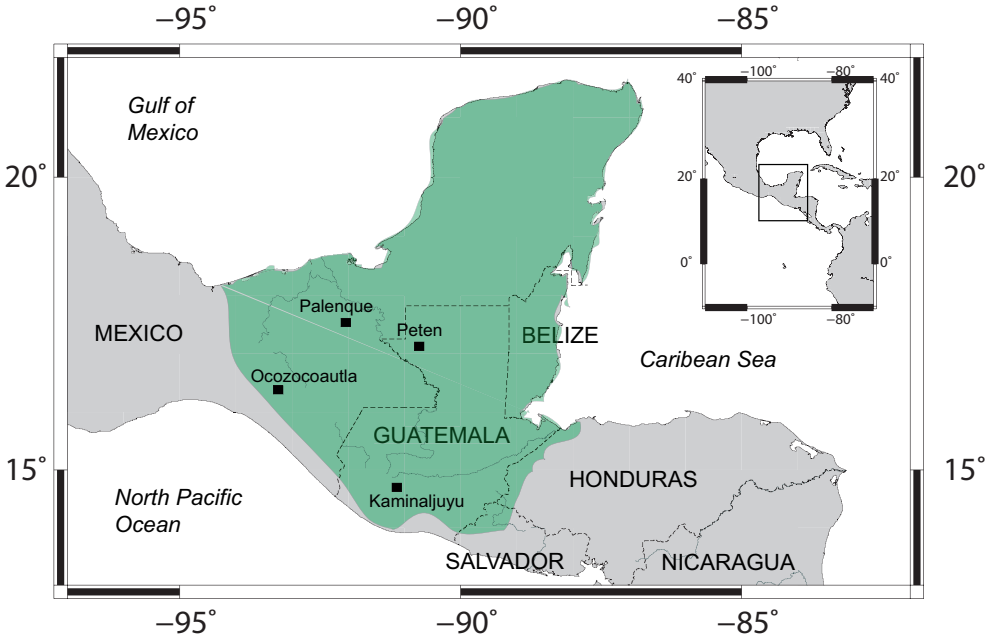

FIGURE 2.17 – *Location map of the Palenque region, Chiapas, Mexico.*

The discovery of about one hundred effigy incense burners in the group of Temples of the Cross in Palenque is an unprecedented event on the Mayan area. Most of them were found buried in the basement of the main temples : the Temple of the Cross, the Temple of the Foliated Cross, and the Temple of the Sun. The other part of censers were found in the architectural complex composed of the temples XIV and XV and Group XVI. Buried censers have been partly altered because of the absence of container and many pieces were broken.

Incense burners were used to worship the gods who were represented on the pedestal by burning vegetable resins and probably human blood deposited in the braziers placed above. Through analysis of the archeological context, one could understand that burying the incense burners representing the gods of the Triad (GI, GII, GIII) in the temples was a ritual practice of periodic renovation. This interpretation results from an ethnographic analogy relying on the study of ritual systems in Palenque and new sight-reading inscriptions (Cuevas-García, 2007). Incense burners show important symbolic properties as the fact of considering the "incense-gods" as living beings having a life cycle. Through their death and resurrection, the regeneration of the world became favorable.

Iconographic, morphological and stylistic analyses, depending on their provenance and manufacturing technology, helped to understand their evolution during the Classic

FIGURE 2.18 – *Two incense burner pedestals from a) Temple of the Foliated Cross (sample TCF-13/93, Balunte) and b) Temple of the Cross (sample TC-5/93, Otulum), from (Cuevas-García, 2007)*

period (200-820 A.D.). During this period, the incense burners were produced continuously and changes in style can be established by means of criteria of evolution, the simplest artifacts attached to the earlier period and the more evolved attached to the most recent period (Cuevas-García, 2007). The most obvious principle is the height of the pedestals and as a consequence, the increase of the number of iconographic patterns (Fig. 2.18). Applying such criteria, Cuevas-García (2007) has established a classification of the censers of Palenque (Fig. 2.16). The Classic period in Palenque is usually divided in 5 or 6 phases. The early Classic is divided into two complexes, Picota (200-350 A.D.) and Motiepa (350-500 A.D). A Middle Classic Cascadas (500-580 A.D.) complex was later added as a subcomplex, but is still debated (Rands, 2007). The Late Classic is composed of three complexes : Otulum (580-680 A.D.), Murcielagos (680-750 A.D.) and Balunté (750-800 A.D.). The main characteristics for each ceramic phases are the following :

1. Motiepa (350-500 A.D.) : The incense burners share an identical manufacturing technique on the basis of a paste of calcite temper and dark color on the inside and brown outside. The size of objects is about 51 cm. In the iconographic motifs the deity known as GI is always represented, accompanied at the top of the head of a

lizard.

2. Cascadas (500-580 A.D.) : The incense burners from this phase are more numerous and are more heterogeneous than those of the previous group, especially with the use of different kind of pastes. They present a greater height, of at least 61 cm and reaching 78 cm. Some modifications in the manufacturing technique are noticed, as the use of different pastes than the incense burners of the Motiepa phase. The god GI is still represented on the pedestal and the GIII deity is introduced. Another distinctive feature arises from the representation of the cheekbones highlighted in the faces of the deities.
3. Otulum (580-680 A.D.) : This set of incense burners is quite homogeneous and show little variability. It appears that there was a hiatus in the manufacturing techniques between Cascadas and Otulum ceramics. The same manufacturing technique was used, but an important increase of the height of the pieces to an average of 81 cm is observed. The GI and GIII are still represented but two variants are introduced, localized only in the Temple of the Cross, while in the Foliated Cross the same variant of the GIII initiated in Cascadas was kept.
4. Murcielagos (A.D. 680-750) : It is a heterogeneous group of incense burners. The manufacturing technique is different of the one used in the previous phases and allows a greater volume of the masks and an higher shape, up to more than 94 cm high. Moreover, different kind of pastes were used and one of them is very crumbly.
5. Balunté (A.D. 750-820) : All censers from this phase share the same manufacturing technique and stylistic similarities, with the representation of the same deities, including variations relative to each temple. These incense burners are the larger pieces and reach 1.14 m in height.

The samples used for the archeointensity study are small non-oriented pieces that have not been reassembled taken from 24 different censers excavated in the Temple of the Cross (13 pieces), Temple of the Cross Foliated (7 pieces), Temple of the Sun (3 pieces) and Group XVI (1 piece). Each piece have been replaced in a ceramic phase (Cuevas-García, 2007), with the archeological arguments described above (Fig. 2.16). For each of them, six small samples (about 5x5x5 mm) were removed and packed in salt pellets in order to treat them as standard paleomagnetic samples and to proceed to archeointensity experiments.

2.4.3 Magnetic properties of samples

A good knowledge of the nature, the size and the thermal stability of the thermoremanence carriers present in the samples is essential prior to any attempt to estimate the archeointensity.

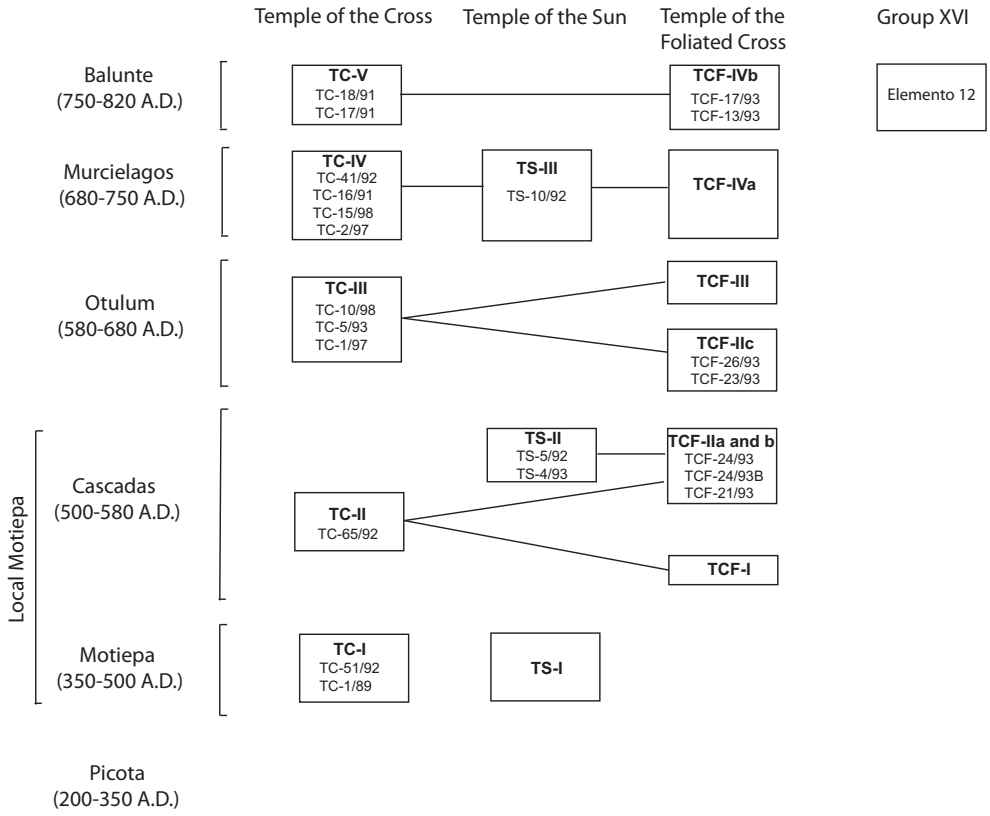

FIGURE 2.19 – *Schematic classification of the censers of the group of temples of Las Cruces (redrawn from Cuevas-García (2007); Rands (2007)).*

Thermomagnetic curves

Low-field susceptibility versus temperature experiments (K-T curves) allow to determine the Curie temperature and the stability of the magnetic carriers upon heatings. Thermomagnetic curves have been performed for at least one piece from each incense burner at the University of Montpellier. First, a piece of archeological material was crushed in an agate mortar and sieved to collect the 0.4-0.8 mm size fraction. Then, K-T curves were acquired at low-temperature by means of a cryostat apparatus (CS-L) and at high-temperature under Argon using a furnace (CS-3) coupled to the KLY-3 Kappabridge instrument (Agico, Czech Republic). The studied material was first heated from liquid nitrogen temperature (78 K) to about 650°C and cooled down to room temperature. Finally the low temperature measurements were repeated from 78 K up to room temperature in order to see if any change occurred. The data were corrected for the empty holder and normalized to the maximum susceptibility. Some samples were treated with several heating-cooling cycles in which the maximum temperature is progressively increased. This procedure allows to estimate the maximum temperature at which the samples can be heated without changing their magnetic properties. Distinct behaviors where identified (Fig. 2.20 a, b, and c). In spite of different shapes, most of the curves

are nearly reversible suggesting few mineralogical changes during heating at least up to 400°C (Fig. 2.20, d). Curie temperatures were calculated using the method of second derivative and vary between 500 and 580°C. This indicates that magnetite or Ti-poor titanomagnetite are the main magnetic carriers. On the contrary, K-T curves from few samples, for example TC Pasta 5 (Fig. 2.20), are not reversible and indicate that these samples are not stable against heating at high temperature.

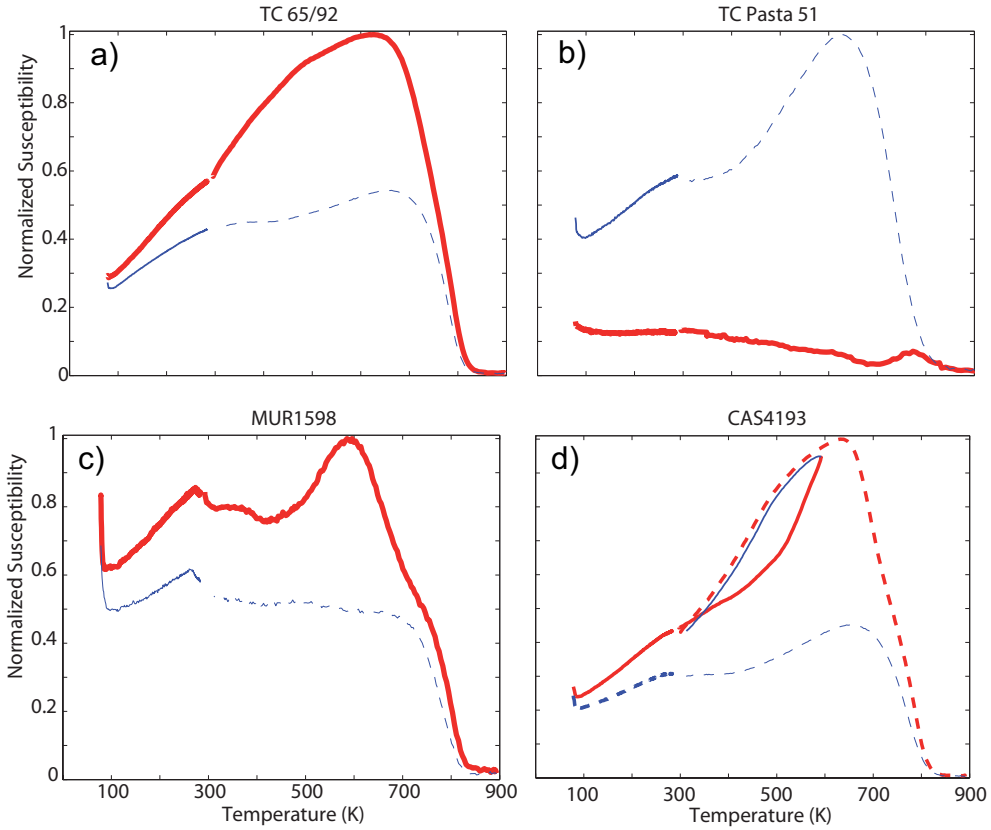

FIGURE 2.20 – *Thermomagnetic curves (a,b,c) and their respective demagnetization curves fro samples TC-65/92, TC Pasta 51 and MUR-15/98. The first heating from liquid nitrogen temperature (78 K) is the thick black curve and the second heating is the fine grey curve. The dashed line is the cooling part of the experiment.*

2.4.4 Hysteresis loops

Hysteresis measurements were performed at room temperature and in fields up to 1.2 T on all studied archaeological pieces by means of the AGFM 'Micromag' apparatus of the paleomagnetic laboratory at Mexico City. The curves are symmetrical in all case and were corrected from the paramagnetic fraction, assuming the absence of magnetic mineral of high coercivity (hematite for example), that is in agreement with the K-T curves. The hysteresis parameter ratios are plotted in the Day diagram (Day et al. (1977), Fig. 2.21). All samples present a pseudo-single domain (PSD) behavior.

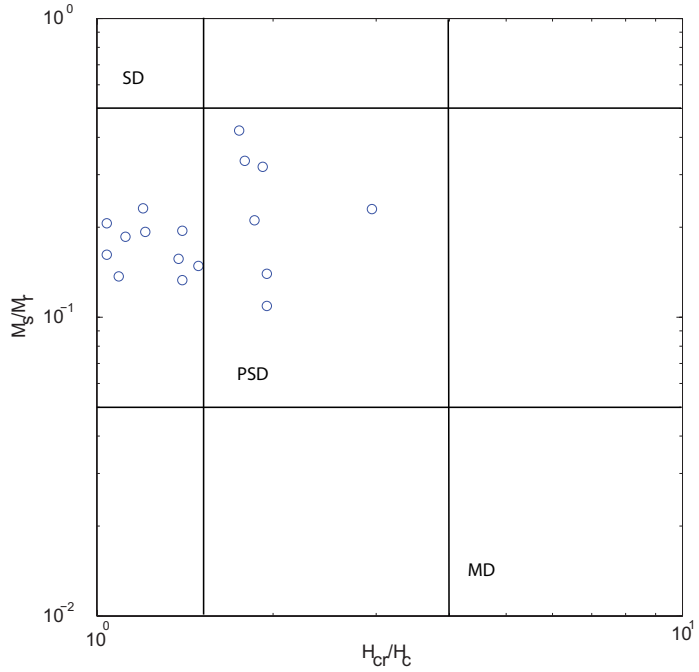

FIGURE 2.21 – Room temperature hysteresis parameters plotted as a Day plot. Ms is tyhe saturation magnetization, Mr is the remanent magnetization, Hc is the coercivity and Hcr is the remanent coercivity.

2.4.5 Firing conditions

Identifications of firing conditions of the samples is an important criterion in order to validate our archeointensity measurements and can bring new insights into the Maya technology. In order to determine firing conditions of our incense burners, three representative samples (Pasta -51, TC 65/94 and TC-41/92) were analyzed by means of X Ray Diffraction Powder (XRPD) and Mössbauer spectroscopy.

X-Ray diffraction powder

The presence or absence of specific mineral assemblages determines the degree of thermal transformation which has occurred in the clay paste of ceramics during the firing. As a consequence the firing temperature during the procedure can be estimated by means of XRPD, revealing either the presence of primary minerals representative of their raw materials or the crystallization of new high-temperature minerals (e.g. Maggetti (1981); Cultrone et al. (2001); Maritan et al. (2006); Rathossi et al. (2011)). A multichannel high performance sequential Wavelength Dispersive X-Ray Fluorescence (WDXRF) spectrometer (Axios 2005, PANalytical, Netherlands) was used. The WDXRF allowed rapid and accurate elemental analysis. The X-ray tube in the present WDXRF spectrometer had Rh anode and operated at a maximum power of 4 kW and a maximum current of

160 mA. For each sample, the characteristic radiation of the major, minor and trace elements were recorded under vacuum in 14 different scans. Each scan covers a certain number of the expected elements and the peak areas of the characteristic radiation were measured. Gas proportional (Ar/CH4) and scintillation counters were used for recording the intensities of the characteristic radiations. Visual inspection of samples permits to distinguish quartz grains that have been removed prior to XRPD analyses. Despite this precaution, powder diffraction patterns of the samples reveal that the main crystallized phase remains unambiguously quartz (Fig. 2.22). The diffraction peaks not belonging to quartz are generally broadened or of very low intensity making difficult their reliable assignment. The absence of primary clay minerals such as illite, smectite or calcite or few remains of muscovite and the presence of high-T new phases such as K-feldspar or anorthite are arguments in favor of a firing temperature up to 800°C (Cultrone et al., 2001; Maritan et al., 2006).

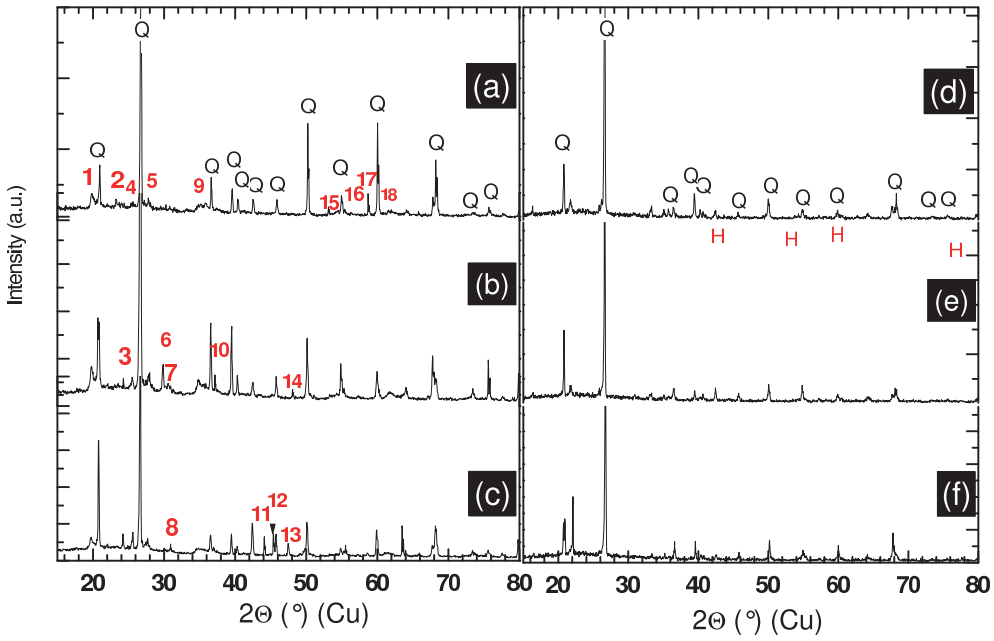

FIGURE 2.22 – *Powder XRD patterns for the samples 1, 2 and 3 before (a, b and c respectively) and after heat treatment at 1100°C (d, e and f). Minerals associated to each peak : Albite (2, 3, 5, 7, 9, 14), Anorthite (5, 7, 9), Anorthoclase (2, 5, 8, 9, 11, 17, 18), Hematite (H), Maghemite (1, 2, 4, 6, 9, 11), Magnetite (7, 9, 10, 15, 18) Muscovite (1, 3, 9, 16, 18), Phlogopite (3, 7, 9, 13, 18), Quartz (Q)and Kaolinite (1, 4, 9, 16, 18).*

Mössbauer spectroscopy

Several Mössbauer studied have shown that either the value of the quadrupole splitting or the relative amount of magnetic and non-magnetic iron can give a clear indication on the firing temperature used for the preparation of ceramics (Murad and Wagner, 1989, 1998; Wagner et al., 1998a; Ricciardi et al., 2008). To get better insight on the nature of

iron in these samples and obtain indication on the firing temperature, Mössbauer spectra have been recorded at room temperature (Fig. 2.23, a to c). The spectra were recorded in transmission geometry with a constant-acceleration spectrometer which utilized a rhodium matrix ^{57}Co source calibrated at 295 K with α-iron foil. The obtained data indicate that all the samples contain iron in the magnetic and non-magnetic states. The samples differ by the relative amount of iron in magnetically ordered state (40, 20 and 15 % for samples Pasta -51, TC 65/94 and TC-41/92 respectively). The best fit of the spectrum is obtained by considering two doublets for the non-magnetically ordered iron and two sextets ordered. The non-magnetic iron is in the ferric state with a wide distribution of sites symmetries since the quadrupole splitting varies from 0.7 to 1.6 mm/s. The two sextets indicate the presence of magnetite and probably some maghemite (Dyar et al., 2006). In this case one can conclude that paramagnetic iron is mainly Fe3+ in octahedral environments with more or less distorted sites. Concerning the magnetic part, the values of the hyperfine field (45-52 T) suggest the presence of phases such as magnetite, hematite and maghemite (McCammon, 1995). As the value of the quadrupole splitting is more model-dependent than the amount of magnetic and non-magnetic iron, it is more reliable to use the later for the estimation of the firing temperatures. Comparing our data to those reported by Murad and Wagner (1989), we can estimate the initial firing temperatures of our samples to be 850, 900 and 1000°C for samples TC41/92, TC65/94, and Pasta 51, respectively (Fig 2.24), in agreement with the XRPD observations.

Firing experiments

In order to check the firing temperature estimations, samples were fired at 1100°C for 10h under air to compare changes occurring in the mineralogy. The obtained products have similar colors. The XRD patterns and Mössbauer spectra are given in Fig. 2.23 and in Fig. 2.22 (d to f). As for the original samples, the patterns of the fired samples are mainly composed of quartz. Very slight modifications are observed ; hematite appeared at the expense of many minor peaks that have disappeared after firing. Mössbauer data show an increase of the magnetic ordered part for all the samples. In the same time, one of the non-magnetic doublets decreases significantly indicating that firing induces the transformation of non-magnetic phases to magnetic ones. Replacing our new values in Fig. 2.24, we estimated the new firing temperature between 1000 and 1100°C, that corresponds to the experimental heating temperature. Thus we conclude that our first estimation of the firing temperatures was quite accurate and that Mayan ceramics were fired in ovens where the temperature was comprised between 850 and 1000°C.

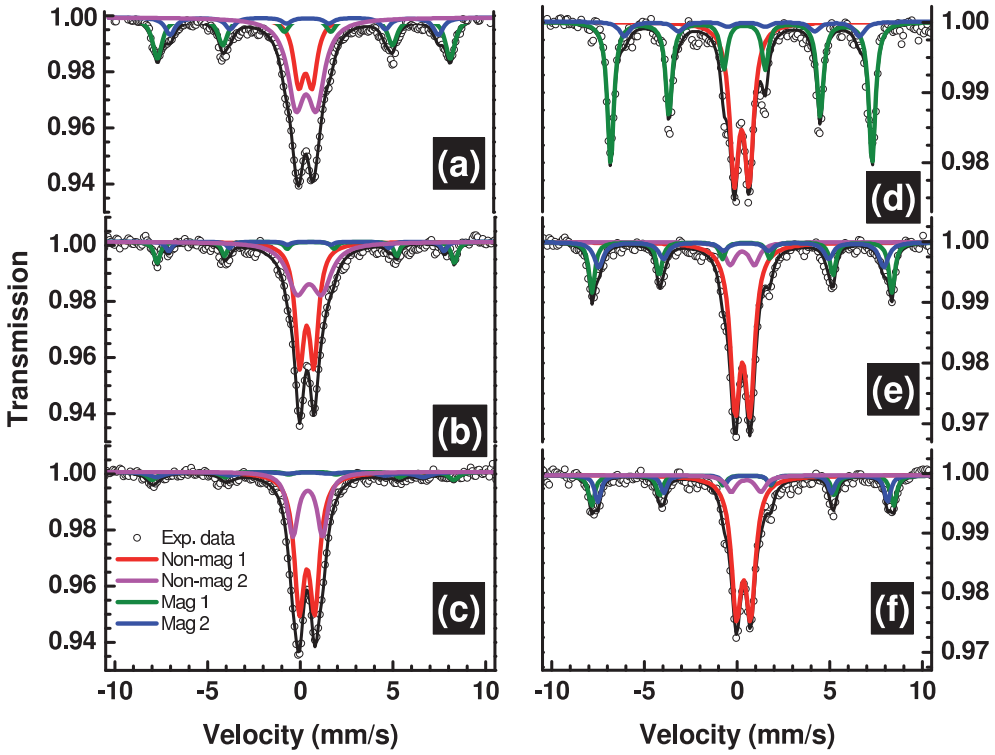

FIGURE 2.23 – *Room temperature Mössbauer spectra of sample 1, 2 and 3 before (a to c) and after firing (d to f).*

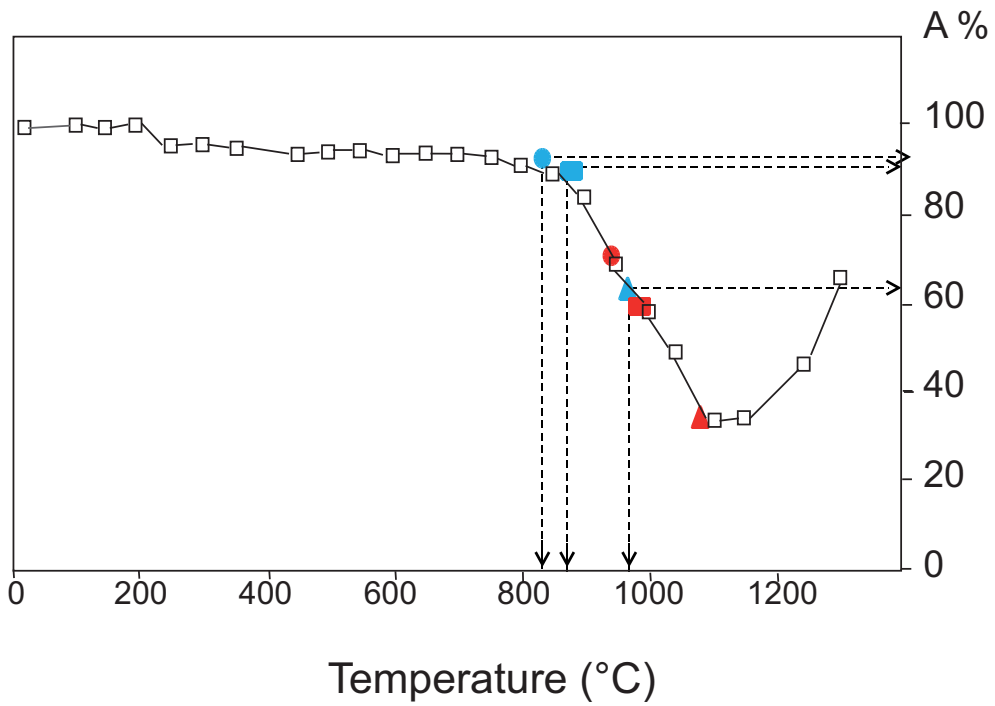

FIGURE 2.24 – Estimated firing temperature based on the non-magnetic iron (right axis). Figure adapted from Murad and Wagner (1989). Pasta 51 : triangle, TC65/94 : squares and TC41 : circles. Blue symbols : before lab firing, red symbols : after lab firing.

2.4.6 Archeointensity determinations

Archeointensity measurements were carried out in the laboratory of Geosciences Montpellier, using the Thellier and Thellier (1959) procedure in its original form, with regular partial thermoremanent magnetization check (pTRM check).

Sample selection

Samples used for absolute archeointensity determinations must satisfy the following criteria :

1. The characteristic remanent magnetization (ChRM) must be a TRM not overprinted by a significant secondary component.
2. The magnetic properties of the samples must be reasonably stable during experimental heatings in the laboratory.
3. The magnetic carriers must be SD or PSD grains in order to fulfill the independence and additivity laws of partial Thermo-Remanent Magnetization (pTRM) (Thellier and Thellier, 1959).

According to the hysteresis parameters, magnetic carriers of most of samples are PSD. Then, according to K-T curves, we selected samples presenting a stable behavior against the temperature to minimize thermal alteration occurring during the successive heatings.

Experimental procedure

Samples were heated and cooled twice for each temperature step T_i. At each temperature level T_i, the samples were cooled in presence of a 40-μT induction field oriented along the z-axis of the core during the first cooling and in the opposite direction during the second one. Temperature steps were performed from room temperature to a maximum temperature of 500°C. Every two temperature increments, a pTRM check was performed to detect any alteration in the pTRM acquisition capacity. All heating-cooling cycles were performed in air. In our paleointensity furnace, the temperature reproducibility between heatings at the same step is within 1°C, and the intensity of laboratory field is maintained with a precision better than 0.1 μT (Camps et al., 2011). After each heating-cooling cycle, the remanent magnetization was measured with a 2G cryogenic magnetometer.

Anisotropy correction Archeomagnetic materials such as pottery, ceramics or bricks are often characterized by a strong magnetic anisotropy (e.g. Aitken et al. (1981); Veitch et al. (1984)). So, the strength of the artificial TRM acquired in the laboratory is dependent on the direction along which the magnetic field is applied. Unless the magnetic field is applied along the direction of the ancient field, an error will be introduced in the

determination of the archeointensity. The importance of this error depends directly on the degree of anisotropy of the sample and on the relative orientations of the ancient field and the laboratory field with respect to the principal anisotropy axes. In order to correct this bias, it is necessary to determine the anisotropic tensor for each sample. Chauvin et al. (2000) have shown that anisotropies of the magnetic susceptibility (A-MS), of the Anhysteretic Remanent Magnetization (A-ARM), and of the Thermo-Remanent Magnetization (A-TRM) present the same orientation of their principal axes but their shapes vary. We choose to correct our archeointensity measurements by means of the anisotropy of TRM. The A-TRM tensor (T) was determined at 290°C. The samples were remagnetized at this temperature in +X, -X, +Y, -Y, +Z, and -Z directions. All archeointensity values were corrected for the A-TRM according to the Veitch et al. (1984)'s method, which consists to first calculate the direction of the ancient field $\mathcal{H}_{anc}$ as :

$$\mathcal{H}_{anc} = \frac{T^{-1} \cdot M_{ChRM}}{|T^{-1} \cdot M_{ChRM}|} \tag{2.5}$$

where M_{ChRM} is the direction of the characteristic magnetization in sample coordinate obtained from the paleointensity determination. The scaling factors for TRM anisotropy correction is given by :

$$\mathcal{F}_{aTRM} = \frac{|T \cdot \mathcal{H}_{lab}|}{|T \cdot \mathcal{H}_{anc}|} \tag{2.6}$$

where $\mathcal{H}_{lab}$ is the laboratory field applied along the core z-axis. Then, the A-TRM corrected archeointensity H_{aTRM} is given by :

$$H_{aTRM} = \mathcal{F}_{aTRM} \cdot H \tag{2.7}$$

where H is the uncorrected archeointensity.

Cooling rate correction The effect of the cooling rate (CR) on the acquisition of a TRM was first reported by Néel (1955) and later by Dodson and McClelland (1980) and Walton (1980), before to be applied to archeomagnetism (e.g. Fox and Aitken (1980); McClelland-Brown (1984)). For baked clays carrying single domain magnetic grains, the TRM acquired during a fast cooling as occurring during laboratory experiments is lower than the one acquired during a slow cooling as occurring in the archeological furnaces. The effect of the CR on our samples was evaluated using the experimental procedure of Chauvin et al. (2000). First, two heating-cooling cycles were performed at the temperature of 220°C using a slow and a fast cooling rate : TRM_1 is the TRM acquired during a fast cooling (3h) and TRM_2 is the TRM acquired during a slow cooling (12h). The effect of the cooling rate was calculated by the ratio $\mathcal{F}_{CR}$ defined as :

$$\mathcal{F}_{CR} = \frac{TRM_2}{TRM_1} \tag{2.8}$$

Then a third TRM, TRM3, was acquired by the samples by means of the same procedure as the initial one, using the same cooling rate. Changes in the TRM acquisition of the samples was evaluated by the ratio $\mathcal{F}_{CR2}$ defined as :

$$\mathcal{F}_{CR2} = \frac{TRM_3}{TRM_1} \tag{2.9}$$

which traduces the alteration of the magnetic carrier properties. For each sample, we compared both factors. The CR correction was considered significant and thus applicable only if $\mathcal{F}_{CR} > 1$ and if the ratio $\mathcal{F}_{CR2}$ was close to 0 or lower than $\mathcal{F}_{CR}$. The corrected archeointensity is given by :

$$H_{aTRM,CR} = \frac{H_{aTRM}}{\mathcal{F}_{CR}} \tag{2.10}$$

Archeointensity results

Archeointensity data were interpreted by means of the Thellier-tool software provided by Leonhardt et al. (2004). We adopted a standard set of criteria derived from those of Selkin and Tauxe (2000) and based on the statistical parameters introduced by Coe et al. (1978) and modified by Prévot et al. (1985) in order to interpret each individual archeointensity data and filter out those of poor technical quality.

1. Archeointensity measurements are represented with Arai's diagram in which the remaining NRM is plotted against the pTRM acquired after each heating step. The slope of the least-squares-fit line computed from the linear part of the diagram gives an estimate of the archeointensity. A value is accepted when the linear segment is defined by more than four points (n>4) and spans over 30% of the total NRM (f>0.3).
2. pTRM checks estimate the thermal alteration of the magnetic properties for each sample and assess the reliability of the archeointensity. We quantified the difference between two pTRM acquisitions at the same temperature using the Difference Ratio (DRAT) parameter. DRAT corresponds to the maximum difference measured in percent between two repeated pTRM acquisition normalized by the length of the selected NRM-TRM segment. We fixed arbitrarily an acceptable threshold at 10%.
3. Finally we checked on the Zijderveld plots computed from the archeointensity measurements that the NRM fraction used to calculate the archeointensity may correspond to the ChRM. The low-temperature part of the NRM may contain natural secondary magnetizations, and at high temperature a chemical remanent magnetization may be acquired during the laboratory heating. This check is performed qualitatively by a visual inspection of the vector endpoint diagrams. The points in the selected interval should trend toward the origin if the NRM is the ChRM.

2.4.6 Archeointensity determinations

TABLE 2.3 – *Archeointensity results n is the number of points in the interval of temperature Tmin-Tmax used to determine the paleointensity ; The fraction of NRM (f), the gap factor (g), and the quality factor (q) were calculated according to Coe et al. (1978) ; DRAT corresponds to the difference ratio between repeat pTRM steps normalized by the length of the selected NRM-pTRM segment ; H is the uncorrected paleointensity estimate for individual specimen and uncertainty ;* $\mathcal{F}_{aTRM}$ *and* $\mathcal{F}_{CR}$ *are the scaling factors for TRM anisotropy and cooling rate corrections, respectively ; the weighted averages for uncorrected paleointensities H, ATRM corrected paleointensities* H_{aTRM}*, and ATRM plus cooling rate corrected paleointensities* $\mathrm{H}_{aTRM,CR}$ *are calculated using* $1/\sigma^2$ *as the weighting parameters. Uncertainties around the estimate of the means are quoted with standard errors.*

Sample	n	T°C min-max	f	g	q	DRAT %	H μT	$\mathcal{F}_{aTRM}$	H_{aTRM} μT	$\mathcal{F}_{CR}$	$\mathrm{H}_{aTRM,CR}$ μT
Balunte A.D. 750-820											
TC :18/91-2	14	20-400	0.65	0.90	10.6	3.9	35.5±1.9	n.d.	n.d.	(0.965)	n.d.
-3	10	100-330	0.68	0.86	14.6	3.0	38.8±1.6	0.743	28.8±1.2	1.007	28.6±1.2
-4	9	130-330	0.66	0.83	80.8	2.0	29.2±0.2	1.074	31.4±0.2	1.007	31.1±0.2
TC :17/91-3	8	140-380	0.72	0.81	18.7	7.8	46.3±1.4	0.807	37.3±1.1	1.042	35.9±1.1
-4	10	100-440	0.77	0.87	13.6	8.7	37.0±1.8	0.969	35.9±1.7	1.012	35.4±1.7
-5	12	100-500	0.95	0.89	8.9	5.9	41.4±3.9	0.814	33.7±3.2	(0.990)	33.7±3.2
-6	8	100-355	0.65	0.81	9.1	8.9	38.3±2.2	0.989	37.9±2.2	1.033	36.7±2.1
El 12 Gpo XVI-1	7	20-400	0.82	0.76	12.9	5.2	31.9±1.6	0.980	31.3±1.6	n.d.	n.d.
-2	10	130-350	0.69	0.87	35.1	1.8	30.1±0.5	1.050	31.6±0.5	1.003	31.5±0.5
-3	10	100-330	0.73	0.87	48.9	0.9	28.9±0.5	1.093	31.6±0.5	1.013	31.2±0.5
-4	11	100-350	0.78	0.87	46.6	1.1	37.1±0.5	0.943	35.0±0.5	(0.998)	35.0±0.5
-5	8	100-355	0.78	0.82	45.1	1.6	29.4±0.4	1.045	30.7±0.4	1.042	29.5±0.4
-6	9	100-380	0.82	0.81	30.1	4.8	32.3±0.7	n.d.	n.d.	1.029	n.d.
TCF :17/93-2	12	130-400	0.68	0.90	17.6	4.2	37.4±1.3	0.827	30.9±1.1	1.007	30.7±1.1
-3	13	130-440	0.72	0.90	34.7	8.0	40.2±0.8	0.921	37.0±0.7	1.009	36.7±0.7
-4	13	100-400	0.62	0.90	22.0	2.2	39.8±1.0	0.816	32.5±0.8	(0.980)	32.5±0.8
TCF :13/93-2	13	100-400	0.80	0.90	21.8	4.9	35.5±1.2	0.894	31.7±1.1	(0.997)	31.7±1.1
-3	16	100-500	0.88	0.92	69.4	4.0	38.7±0.4	0.822	31.8±0.3	(0.962)	31.8±0.3
-4	10	100-330	0.75	0.87	22.6	5.4	38.0±1.1	n.d.	n.d.	1.004	n.d.
						unweighted average :	36.1±1.1		33.1±0.7		32.8±0.7
						weighted average :	32.0±1.4		32.0±0.7		**31.7±0.7**
Murcielagos A.D. 700-750											
TC :41-1	6	120-400	0.68	0.74	6.9	4.9	38.6±2.9	0.838	32.3±2.4	n.d.	n.d.
-2	12	130-400	0.52	0.88	14.9	7.5	34.0±1.0	0.911	31.0±0.9	(0.991)	31.0±0.9
-3	9	160-350	0.56	0.85	20.1	1.5	39.0±0.9	0.824	32.1±0.7	1.007	31.9±0.7
-4	13	100-400	0.79	0.89	20.4	5.7	36.3±1.3	0.848	30.8±1.1	(0.985)	30.8±1.1
TC :16/91-4	11	180-500	0.76	0.87	12.0	9.9	39.8±2.2	0.766	30.5±1.7	1.000	30.5±1.7
TC :15/98-3	11	180-500	0.69	0.89	31.0	2.2	43.8±0.9	0.777	34.0±0.7	1.009	33.7±0.7
TS :10/92-2	15	130-500	0.86	0.92	44.7	5.0	35.2±0.6	0.910	32.0±0.5	1.012	31.7±0.5
-3	16	100-500	0.87	0.92	50.1	4.8	32.6±0.5	0.898	29.3±0.4	1.019	28.7±0.4
-4	16	100-500	0.85	0.92	71.6	5.2	36.6±0.4	0.834	30.5±0.3	1.013	30.1±0.3
						unweighted average :	37.3±1.1		31.4±0.5		31.0±0.5
						weighted average :	36.0±1.2		30.9±0.5		**30.5±0.6**
Otulum A.D. 620-700											
TC :10/98-4	11	180-500	0.86	0.87	19.8	4.3	38.7±1.5	0.883	34.2±1.3	(0.960)	34.2±1.3
-5	13	100-500	0.84	0.87	32.4	1.7	45.0±1.0	0.839	37.8±0.8	(0.980)	37.8±0.8
-6	12	100-470	0.88	0.87	15.5	4.6	38.2±1.9	0.810	30.9±1.5	(0.978)	30.9±1.5
TC :5/93-4	11	180-500	0.86	0.85	30.4	2.5	39.4±1.0	n.d.	n.d.	1.000	n.d.
-5	13	100-500	0.84	0.87	31.7	5.0	31.8±0.7	0.911	29.0±0.6	1.000	29.0±0.6
-6	13	100-500	0.85	0.88	36.4	3.9	36.0±0.7	0.900	32.4±0.6	(0.996)	32.4±0.6
TC :1/97-5	8	255-470	0.66	0.81	38.8	2.8	37.5±0.5	0.816	30.6±0.4	(0.965)	30.6±0.4
-6	10	220-500	0.77	0.85	34.7	1.7	45.7±0.9	0.734	33.5±0.7	(0.986)	33.5±0.7
TCF :26/93-3	8	100-355	0.68	0.83	30.9	2.8	29.8±0.6	0.912	27.2±0.5	1.043	26.1±0.5
-4	7	140-355	0.67	0.82	30.3	1.3	34.2±0.6	0.916	31.3±0.5	1.037	30.2±0.5
-5	13	100-500	0.90	0.90	14.2	5.4	33.4±1.9	0.809	27.0±1.5	1.013	26.7±1.5
						unweighted average :	37.2±1.5		31.4±1.0		31.1±1.1
						weighted average :	36.0±1.6		30.9±1.1		**30.5±1.1**

All archeointensity determinations are gathered in Table 2.3 and 2.4 and a qualitative appreciation of the results is given for samples from two incense burners on Fig. . The scaling factors used to correct the measured paleointensities for the cooling rate ($\mathcal{F}_{CR}$) and anisotropy ($\mathcal{F}_{aTRM}$) effects are reported in Table 2.3. The corrections for cooling rate are rather small with a maximal correction of 9% (Table 2.3). On the contrary, the effect of anisotropy of TRM can be relatively important provided that $\mathcal{F}_{aTRM}$ are in the range of 0,743 to 1,115. Two points deserve to be noted on the importance of A-TRM correction on the final archeointensity results. First, in most cases the corrected archeointensity value is lower than the uncorrected one. Second, uncertainties around

TABLE 2.4 – *End of the archeointensity results.*

Sample	n	T°C min-max	f	g	q	DRAT %	H μT	$\mathcal{F}_{aTRM}$	H_{aTRM} μT	$\mathcal{F}_{CR}$	$H_{aTRM,CR}$ μT
Cascadas A.D. 500-620											
TC :65/92-2	13	190-500	0.76	0.90	24.5	6.3	32.4±0.9	0.840	27.2±0.8	1.009	27.0±0.8
-3	14	160-500	0.82	0.91	33.2	4.0	28.9±0.7	1.050	30.3±0.7	1.014	29.9±0.7
-4	13	190-500	0.76	0.90	41.3	4.0	37.7±0.6	0.819	30.9±0.5	1.016	30.4±0.5
-5	12	140-500	0.82	0.89	31.7	3.0	39.2±0.9	0.947	37.1±0.9	1.003	37.0±0.9
TS :5/92-1	8	120-470	0.82	0.84	7.4	3.7	34.1±3.2	0.998	34.0±3.2	n.d.	n.d.
-2	17	20-500	0.88	0.92	27.5	3.1	31.4±0.9	1.009	31.7±0.9	1.012	31.3±0.9
-3	16	100-500	0.84	0.92	65.5	2.3	40.8±0.5	0.853	34.8±0.4	1.000	34.8±0.4
-4	16	100-500	0.85	0.91	60.0	1.9	31.5±0.4	1.056	33.3±0.4	1.015	32.8±0.4
-5	12	100-470	0.79	0.90	18.3	2.2	31.4±1.2	0.926	29.1±1.1	1.034	28.1±1.1
TS :4/93-2	10	140-440	0.71	0.88	15.7	7.0	44.1±1.8	0.941	41.5±1.7	1.024	40.5±1.7
-3	13	100-500	0.81	0.90	41.5	1.7	42.5±0.8	0.813	34.6±0.7	1.006	34.3±0.7
-4	13	100-500	0.85	0.90	21.1	2.7	38.6±1.4	0.822	31.7±1.2	1.027	30.9±1.2
				unweighted average :			36.1±1.5		32.9±1.2		32.5±1.2
				weighted average :			35.4±1.5		32.8±1.2		**32.5±1.2**
Motiepa A.D. 400-500											
TC : Pasta51-3	9	100-310	0.65	0.86	17.0	1.6	28.6±0.9	1.005	28.7±0.9	1.014	28.3±0.9
-4	13	100-400	0.78	0.91	41.8	3.0	29.5±0.5	0.998	29.4±0.5	1.018	28.9±0.5
-5	10	100-330	0.70	0.88	18.2	2.1	30.0±1.0	1.070	32.1±1.1	1.014	31.7±1.1
-6	9	100-380	0.73	0.84	20.9	6.9	30.8±0.9	1.061	32.7±1.0	1.052	31.1±1.0
TC :51/92-2	13	100-500	0.81	0.90	9.9	4.6	44.3±3.3	0.765	33.9±2.5	1.045	32.4±2.4
-3	7	140-355	0.51	0.83	4.2	9.5	33.8±3.4	0.807	27.3±2.7	1.088	25.1±2.5
-4	10	100-400	0.65	0.86	5.6	7.3	36.9±3.7	0.838	30.9±3.1	1.068	28.9±2.9
-5	10	180-470	0.77	0.88	7.8	3.3	37.4±3.2	0.723	27.0±2.3	1.065	25.4±2.2
-6	9	140-400	0.68	0.87	8.2	5.6	27.2±2.0	0.926	25.2±1.9	1.090	23.1±1.7
TC :1/89-2	14	20-400	0.83	0.90	11.8	6.1	36.3±2.3	0.918	33.0±2.1	1.086	30.7±1.9
-3	9	100-310	0.54	0.83	12.3	9.9	41.0±1.5	n.d.	n.d.	1.076	n.d.
-4	13	160-470	0.79	0.88	8.9	4.8	33.8±2.7	0.843	28.5±2.3	1.041	27.4±2.2
-5	9	140-400	0.64	0.86	10.8	6.2	39.5±2.0	0.902	35.6±1.8	1.066	33.4±1.7
-6	10	100-400	0.67	0.85	7.1	6.8	23.2±1.9	1.115	25.9±2.1	1.007	25.7±2.1
				unweighted average :			33.7±1.6		30.0±0.9		28.6±0.9
				weighted average :			30.7±1.8		30.0±0.9		**29.1±0.9**

the estimate of the means are always lower after than before A-TRM corrections, which is *a posteriori* a good justification to apply this correction.

At the total, we obtained a high success rate, with 19 mean archeointensities determined over the 24 censers and with 9 to 19 samples per ceramic period.

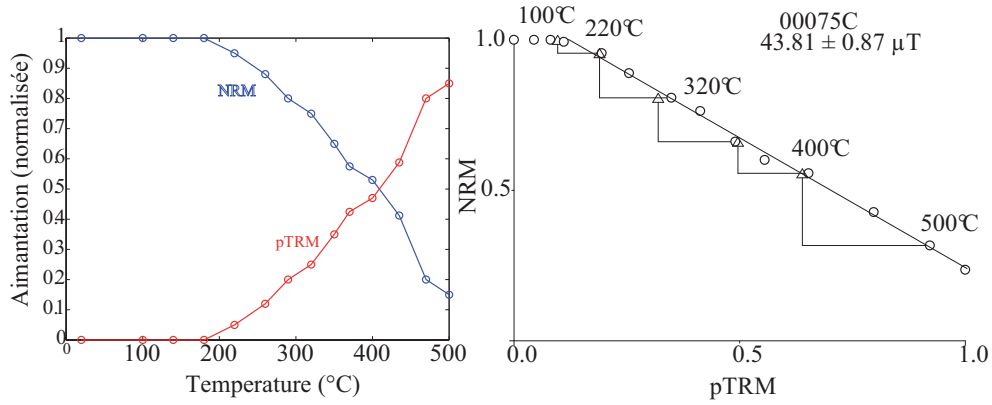

FIGURE 2.25 – *Composite Arai diagrams for samples from Murcielagos epoch (TC : Templo de la Cruz, TS : Templo del sol). Solid (open) circles are NRM-TRM points accepted (rejected) to calculate the least squares line used to estimate the paleointensity. Triangles denote the pTRM checks. NRM and TRM are normalized by the NRM max and TRM max, respectively.*

2.4.7 Discussion

2.4.8 Reliability of the archeintensity determinations

The overall technical quality of the present archeointensities is very good as attested by the quality factors ranging from 6.9 to 80.8. We observed well-defined straight segments on NRM-TRM curves over a large range of NRM fraction ; 66% of archeointensity estimate are calculated with a NRM fraction greater than 40%. In addition, the individual archeointensity estimates are fairly coherent when they are compared within a single ceramic phase. We calculated a weighted average and a standard error average for each phase, using the weighting by the standard error as recommended by Coe et al. (1978). Each mean ceramic phase intensity value was calculated with at least 9 samples and presents a very low standard error lower than 4% about the mean. The X Ray diffraction results and Mössbauer spectra yield additional arguments to validate our archeointensity determinations. These experiments, which are independent of the magnetic remamence properties, concluded for very high firing temperatures during the manufacturing process. Indeed, the initial firing temperatures for all the incense burners, estimated between 850 and 1000°C, are sufficiently high to ensure formation of magnetic minerals and to record during cooling a full TRM. Thus, we believe very reliable this new dataset.

Secular variation during the Classic Period

According to these results, during the Classic period in Mesoamerica, the magnetic field intensity varied slightly, from a minimum of 29.1 ± 0.9 μT during Motiepa to a maximum of 32.9 ± 1.2 μT during Cascadas. This corresponds to a virtual axial dipole moment (VADM) varying from 6.7 ± 0.2x10^{22} A.m^2 to maximum 7.5 ± 0.3x10^{22} A.m^2 during these four centuries. These new archaeointensities are important because they can help to clarify the different ceramic phases. In particular they confirm the chronology of incense burners before the Murcielagos complex, since the presence of objects associated with Motiepa and Cascadas do not present any hieroglyphic inscriptions in the archeological complex of the Cross. Although Cascadas subdivision has been removed from Motiepa phase (Rands, 2007) and that it does not appear in the seriation of the censers, two stages are still identifiable during Motiepa phase (Román, 2005; Rands, 2007). Indeed, incense burners from 400 to 620 A.D. do not form a homogeneous group as they present variations in manufacturing techniques, iconic designs and styles. Such differences may be attributed to the development of these incense burners at different times within this period of 200 years. Moreover our study clearly distinguishes two subdivisions : early Motiepa and late Motiepa (Cascadas) phases. A significant difference in the mean field intensity is observed ; 29.1 ± 0.9 μT during early Motiepa and 32.9 ± 1.2 μT during Cascadas. Thus we can argue in favor of a subdivision of the Motiepa phase

into a early Motiepa phase (400-500 A.D.) and a Cascadas phase (500-620 A.D.).

Comparison with previous data in Mesoamerica and global models

Nowadays, few archeointensities were acquired in Mesoamerica (Mexico, Belize and Guatemala). Despite the study of several sites and periods in the last decade, the regional secular variation curve (SVC) remains poorly defined. We compiled all archeointensity studies carried out in this region on archaeomagnetic artifacts or basalts, by means of all methodology (Thellier-thellier type, Shaw, microwave or multispecimen methods). Donadini et al. (2006) and Korhonen et al. (2008) have developed a database system (GEOMAGIA) to store archeomagnetic data and easily query them at https ://geomagia.ucsd.edu. Recently, this database has been expanded to a larger comprehensive version called MagIC. From this database and including data from our study, 84 data are available from 2750 B.C. to 2012 A.D. for the Mesoamerica area (Fig. 2.26, a). The global models ARCH3k (Donadini et al., 2009) and CALS10k (Korte et al., 2011) are also plotted. A large dispersion of the data is observed, even in the recent time. In order to make a first selection, we used the criteria of Donadini et al. (2009) to build a constrained archeomagnetic dataset. We selected only data with $\sigma_{VADM} < 2\text{x}10^{22}$ A.m^2 and $\sigma_{age} < 100$ years (Fig. 2.26, b). Even with this first selection, the dispersion is still important thought reduced. To investigate the reliability of this data, we choose to impose more drastic selection criteria. Indeed the scatter pattern of data could be explained either by the methodology or by the absence of CR correction and/or A-TRM correction on data obtained from archeological artifacts. The Shaw method (Shaw, 1974) and the multispecimen method (Dekkers and Böhnel, 2006; Fabian and Leonhardt, 2010) are not conventional methods in paleo- and archeo-intensity determinations and can yield significant over- or under- estimations of the intensity. Thus, in order to avoid these two bias, we decided to select only measurements satisfying the following conditions :

1. The data must be obtained by means of Thellier-like methods.
2. If the data was carried out from an archeological artifact, A-TRM and CR corrections should have been applied.
3. An alteration control by means of pTRM checks must have been performed during the experiment.

Our new selection data is plotted on Fig. 2.26, c. Very few data meet all these criteria, which guaranty their technical quality and show a reduced but non neglecting scattering. In this context, our high technical quality data represent a strong constrain for the Mesoamerican secular variation curve. However the few quantity of reliable data do not allow to build a reference regional curve (Lanos et al., 2005) or a regional model (Pavón-Carrasco et al., 2010). More data are required, in particular to confirm the low

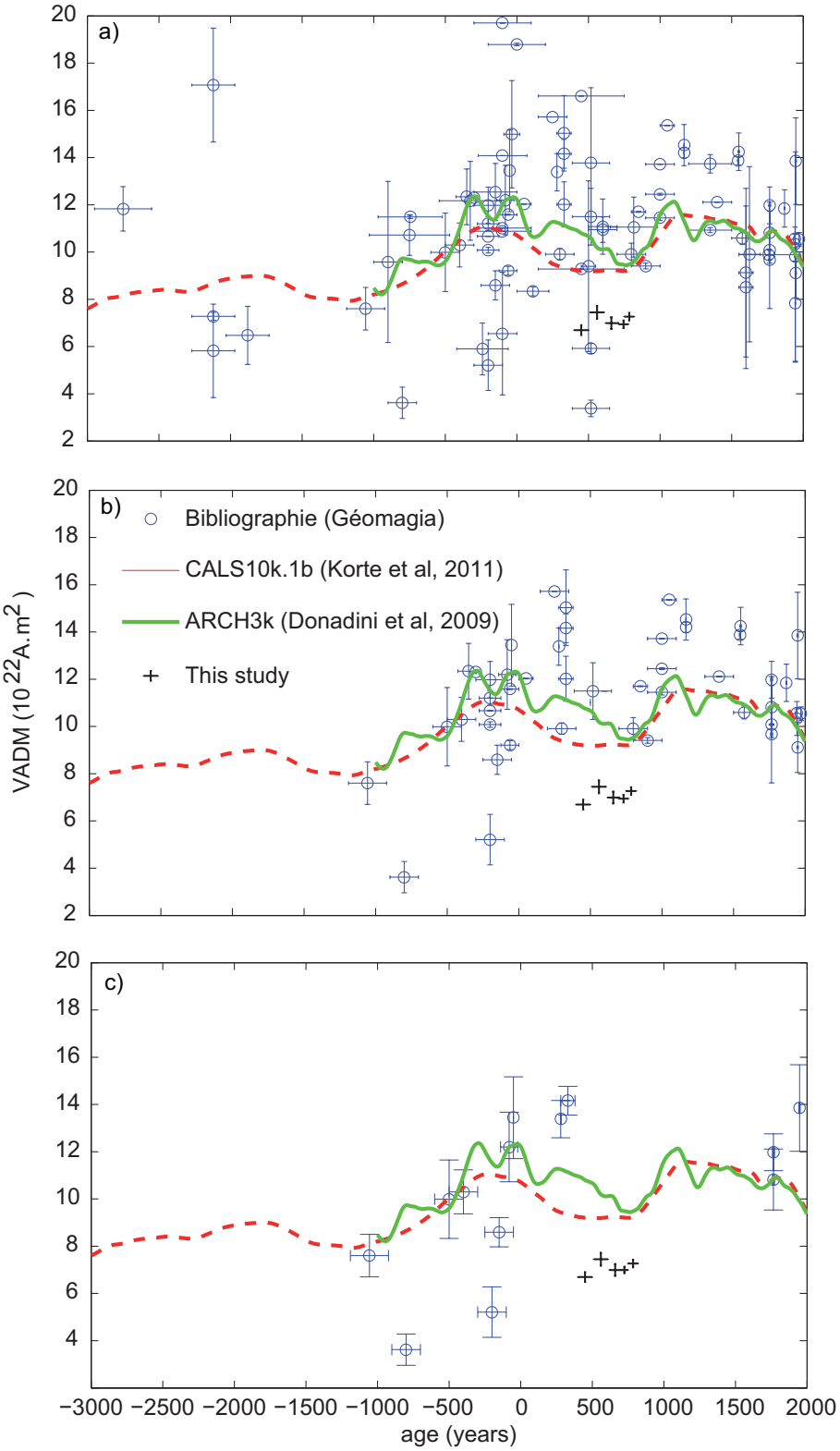

FIGURE 2.26 – *Compilation of archaeintensity VADM data available for Mesoamerica a) All data b) Data selection by means of the Donadini et al. (2009)'s criteria c) Data selection by means of our criteria (see text for explanation).*

VADM values found between 400 and 800 A.D. The Uxmal site located in the center of the Yucatan peninsula appear as the ideal candidate for a next study. Larger numbers of high-quality data will allow the rejection of data of unknown or questionable quality, improving the signal to noise ratio in the global and regional datasets. This step is of first importance to increase global model resolution both in space and time resolution to answers questions of geophysical interests and to enable the development of reliable regional reference curves involved in archeometry dating.

2.4.9 Conclusions

Of the 24 samples from Maya incense burners used to estimate the archeointensity during the Classic Period in the Palenque area, 19 yield a reliable determination. Measurements were performed with the Thellier-Thellier method on pre-selected samples by means of their magnetic properties. We estimated the firing temperature of the ceramics between 850 and 1000°C that ensures that the full TRM was acquired during the manufacturing heating. The present experimental study leads to the following conclusions :

1. The intensity of the Earth's magnetic field varied slightly during the Classic Maya period, from a minimum of 29.1 ± 0.9 μT during Motiepa to a maximum of 32.9 ± 1.2 μT during Cascadas. This corresponds to a VADM varying from 6.7 ± 0.2x10^{22} A.m^2 to maximum 7.5 ± 0.3x10^{22} A.m^2.

2. These new archeointensities help to clarify the different ceramic phases. Indeed, incense burners from 400 to 620 A.D. do not form a homogeneous group as they present variations in manufacturing techniques, iconic designs and styles. Such differences may be attributed to the development at different times within this period of 200 years. Our study clearly argues in favor for a subdivision of the Motiepa phase into a early Motiepa phase (400-500 A.D.) and a Cascadas phase (500-620 A.D.).

3. The abundance of archeological material in this region contrasts with the small amount of archeomagnetic data in Mesoamerica available over the last few millennia. Moreover, these data are also of uneven quality. Thus, it is especially difficult to establish a trend in the intensity variations in the Mesoamerican region, even using the databases in the world and predictions of secular variation of the existing global models. As a consequence our high technical quality data represent a strong constrain in the Mesoamerican secular variation curve. The VADM values found are smaller than the ones predicted by the global geomagnetic models, suggesting the need to develop a regional model for the secular variation curve in Mesoamerica.

2.5 Compléments d'information

2.5.1 Comment obtenir une valeur fiable d'archéointensité en laboratoire ?

Les mesures expérimentales en archéomagnétisme consistent à déterminer la direction et/ou l'intensité du champ magnétique terrestre dans des terres cuites archéologiques. Si ces dernières n'ont pas été déplacées après leur cuisson (comme par exemple une parois de four, briques de four..) on peut à la fois déterminer la direction et l'intensité du champ au moment de la dernière cuisson, dans le cas contraire (comme par exemple des fragments de poterie, céramiques etc...) seule l'intensité pourra être déterminée, exceptée si on connaît leur positionnement exact lors de leur cuisson. Nous nous focaliserons ici sur la détermination d'une archéointensité, la procédure d'obtention des directions étant strictement identique à celles des laves. Pour déterminer une archéointensité, la méthode classiquement utilisée est celle de Thellier ou une de ses dérivées (cf. Annexes 2). Néanmoins, après avoir mené ce protocole, la valeur de l'intensité ainsi obtenue doit être doublement corrigée de deux erreurs introduites par des biais expérimentaux : d'une part par le taux de refroidissement et d'autre part par l'anisotropie d'aimantation thermorémanente (A-ATR).

Correction du taux de refroidissement

L'effet du taux de refroidissement sur l'acquisition d'une ATR a été étudié en premier lieu par Néel (1955), puis plus tard par Dodson and McClelland (1980); Walton (1980); Halgedahl et al. (1980). L'application directe ce travail à l'archéomagnétisme s'est également déroulé au début des années 80 (e.g. Fox and Aitken (1980); McClelland-Brown (1984)). L'ensemble des observations montrent que pour des minéraux monodomaines (ce qui est requis pour appliquer la méthode Thellier), l'ATR acquise au cours d'un refroidissement lent (four archéologique) est plus élevée que l'ATR acquise au cours d'un refroidissement rapide (four expérimental pour mesurer les paléointensités). Aitken (1983) a reporté l'effet des taux de refroidissement sur des poteries qui ont été aimantées puis refroidies lentement pendant deux jours. Les intensités ainsi acquises ont été mesurées en utilisant des temps de refroidissement au sein du laboratoire de 5 min à 4h, entrainant une sur-estimation de 11% et 3 % respectivement. Ainsi, l'erreur due au taux de refroidissement peuvent être relativement conséquentes. Afin de tenir compte de cette possible erreur, trois chauffes à une température donnée sont effectuées (Chauvin et al., 2000). La température doit être suffisamment élevée pour qu'une fraction suffisante d'ATR soit touchée mais assez basse pour éviter une altération possible. La première chauffe se fait dans les conditions classiques de détermination de la paléointensité avec une refroidissement rapide (4h). La seconde acquisition se fait avec un refroidissement lent (environ 12

h) et la troisième de nouveau avec un refroidissement rapide identique au premier. On peut ainsi définir un facteur de correction du taux de refroidissement r_1 (eq. 2.11) et un facteur d'altération r_2 (eq. 2.12).

$$r_1 = \frac{ATR_2 - ATR_1}{ATR_1}, \tag{2.11}$$

$$r_2 = \frac{ATR_3 - ATR_1}{ATR_1} \tag{2.12}$$

Si r_1 et r_2 sont très proches, il est dans ce cas relativement difficile de pouvoir attribuer une correction de taux de refroidissement dans la mesure où l'erreur peut être également attribuée à l'altération. Une seconde correction est également à apporter : la correction d'A-ATR.

Correction du degré d'anisotropie

Les matériaux archéologiques présentent très souvent de fortes fabriques dont l'origine provient de leur mode de fabrication, c'est le cas essentiellement pour les briques, les poteries et les céramiques. Cette fabrique se répercute au niveau magnétique dans la mesure où les matériaux présentent une anisotropie magnétique très marquée (Aitken et al., 1981; Veitch et al., 1984). Ainsi, l'ATR artificielle acquise en laboratoire est directement dépendante de la direction dans laquelle le champ magnétique est appliqué. A moins que ce dernier ne soit appliqué dans la direction du champ magnétique passé enregistré lors du refroidissement du matériau, une erreur sera introduite lors de la mesure de la paléointensité. L'importance de cette erreur dépend à la fois du degré d'anisotropie de l'échantillon et des directions relatives entre les axes principaux du tenseur d'anisotropie et de la direction du champ appliqué Afin de corriger cette erreur, il est nécessaire de mesurer le tenseur d'anisotropie pour chaque spécimen. (Chauvin et al., 2000) a montré que les tenseur d'anisotropie de susceptibilité, de rémanence thermique et et de rémanence anhystérétique avaient tous la même orientation mais que le degré d'anisotropie diffère d'un tenseur à l'autre. Nous avons choisit de corriger nos mesures brutes d'intensité par la mesure d'anisotropie d'ATR, le processus d'acquisition de l'aimantation dans les céramiques étant thermique. La procédure de correction a été développée par (Veitch et al., 1984). L'anisotropie d'ATR est mesurée à des températures moyennes afin de minimiser l'altération tout en travaillant sur une fraction d'aimantation suffisamment importante. Chaque échantillon est soumis à une chauffe puis un refroidissement au cours duquel un champ magnétique est appliqué dans les directions +X,-X,+Y,-Y, +Z et -Z. Ensuite le tenseur d'anisotropie est déterminé puis la le facteur correctif estimé selon la procédure de Veitch et al. (1984). La direction du moment magnétique $\mathbf{m}$ enregistré dans une céramique est dépendant de la direction du champ $\mathbf{H}$ et de la fabrique magnétique :

$$\mathbf{m} = K \cdot \mathbf{H}, \tag{2.13}$$

où (i,j)=(x,y,z,)et K est le tenseur de susceptibilité. Pour des champs faibles, le tenseur est symétrique, d'où $K_{ij} = K_{ij}$. Les mesure d'A-ATRM permettent de déterminer les coefficients K_{ij} du tenseur. Ce tenseur est ensuite diagonalisé, ce qui permet d'obtenir les vecteurs propres, souvent assimilés aux directions des contraintes appliquées lors de la manufacture de l'objet. Le calcul du vecteur unitaire **h**, correspondant à la direction du champ ancien et donnée par l'équation :

$$\mathbf{h} = \frac{K^{-1} \cdot \mathbf{m}}{\|K^{-1} \cdot \mathbf{m}\|}. \tag{2.14}$$

Ensuite, le facteur de correction f_{ATR} est donné par la relation suivante :

$$f = \frac{\|k \cdot \mathbf{u}\|}{\|k \cdot \mathbf{h}\|}, \tag{2.15}$$

où **u** est le vecteur unitaire dirigé selon l'axe z de la carotte, direction d'application du champ en laboratoire.

Le calcul de ces deux paramètres est fondamental pour obtenir une valeur d'archéointensité fiable. La détermination des conditions de cuisson est un autre paramètre qui peut apporter un poids supplémentaire sur la validité des mesures.

2.5.2 Détermination des conditions de cuisson du matériel archéologique

La réaction de durcissement qui a lieu au cours de la cuisson dans les pâtes riches en argiles est un processus fondamental de la technologie de la céramique. Ce processus se produit à haute température et les transformations minérales sont principalement influencées par la composition de la matière première et les conditions de cuisson. La détermination de ces conditions, notamment la température maximale atteinte lors de la cuisson, est un élément important dans une étude archéomagnétique. En effet, si la température atteinte est supérieure à la température maximale de déblocage des minéraux porteurs de l'aimantation, alors l'aimantation portée par la poterie correspond à une ATR dont l'intégralité a été acquise lors de la cuisson. Si ce n'est pas le cas, l'interprétation des résultats est compromise. L'évaluation de la température de cuisson peut être effectuée par l'identification des phases minérales présentes dans l'échantillon. Pour ce faire, deux techniques sont mise en oeuvre : la diffraction des Rayons X (DRX) et la spectroscopie Mössbauer.

Par la spectroscopie de diffraction aux rayons X

La présence ou l'absence d'assemblages de minéraux spécifiques détermine le degré de transformation thermique qui s'est produite dans la pâte d'argile de la céramique au cours de la procédure de cuisson. Ceci permet d'estimer la température de cuisson pendant le fonctionnement des fours (Cultrone et al., 2001; Maritan et al., 2006; Rathossi

and Pontikes, 2010). Des minéraux tels que l'illite (mica blanc) ou la calcite sont des minéraux primaires dont la présence révèle une cuisson à relativement basse température (inférieur à 750°C), comme l'indique l'équation suivante :

$$\underset{\text{(illite)}}{KAl_2(Si_3Al)O_{10}(OH)_2} + 2CaCO_3 + 4SiO_2 \rightarrow \underset{\text{(feldspath-K)}}{2KAlSi_3O_8} + \underset{\text{(anorthite)}}{2Ca_2Al_2SiO_8} + 2CO_2 + H_2O$$

A l'inverse, la présence de feldspaths, pyroxènes, gehlnite ou encore mullite témoignent de températures de cuisson supérieures à 800°C (Cultrone et al., 2001). L'analyse de la diffraction des rayons X sur poudre (DRXP) est souvent utilisé pour la caractérisation minéralogique des échantillons de céramique. Cette méthode consiste en l'étude de la diffraction des Rayons X (DRX) par des solides cristallisés sous forme polycristalline à orientation supposée parfaitement statistique. Le matériau est bombardé par un faisceau de rayons X monochromatiques et parallèles de longueur d'onde connue, produit grâce à une anticathode de cuivre. Le rayonnement émis est défini par un système de fentes et de fenêtres situées avant et après l'échantillon. Ce dernier est étalé sous forme de poudre (15 mg environ) sur une lame de verre qui tourne uniformément autour d'un axe situé dans son plan, permettant ainsi d'augmenter le nombre d'orientations possibles des plans réticulaires. Les particules étant orientées au hasard, il y aura toujours une famille de plans donnant lieu à la diffraction Un détecteur ou compteur (Geiger-Müller ou compteur à scintillation) mesure l'intensité du rayonnement X diffracté dans certaines directions. Il tourne autour du même axe mais à une vitesse double de celle de l'échantillon. Pour un angle d'incidence θ, l'angle mesuré par le déplacement du compteur sera donc 2θ. L'enregistrement réalisé correspond à la courbe de l'intensité des rayons X diffractés en fonction des angles de diffraction mesurés 2θ (Fig. 2.27). La position des pics de diffraction permet l'identification des structures ou phases cristallines présentes et donc la détermination de la composition cristallographique de l'échantillon analysé. Néanmoins, cette méthode ne nous permet pas toujours d'obtenir une réponse précise sur les températures de cuisson atteinte. La spectroscopie Mössbauer peut également apporter des informations complémentaires.

Par la spectroscopie Mössbauer

La spectroscopie Mössbauer, en magnétisme des roches, est utilisée principalement pour distinguer quantitativement les proportions des différents minéraux magnétiques, en distinguant notamment le fer ferreux Fe(II) et le fer ferrique Fe(III). L'effet Mössbauer a été mis en évidence en 1958.

Principe La spectroscopie Mössbauer est basée sur la résonance des atomes au rayonnement γ. Lorsqu'un quanta d'énergie γ est émis par un atome passant d'un état excité

2.5.2 Détermination des conditions de cuisson du matériel archéologique

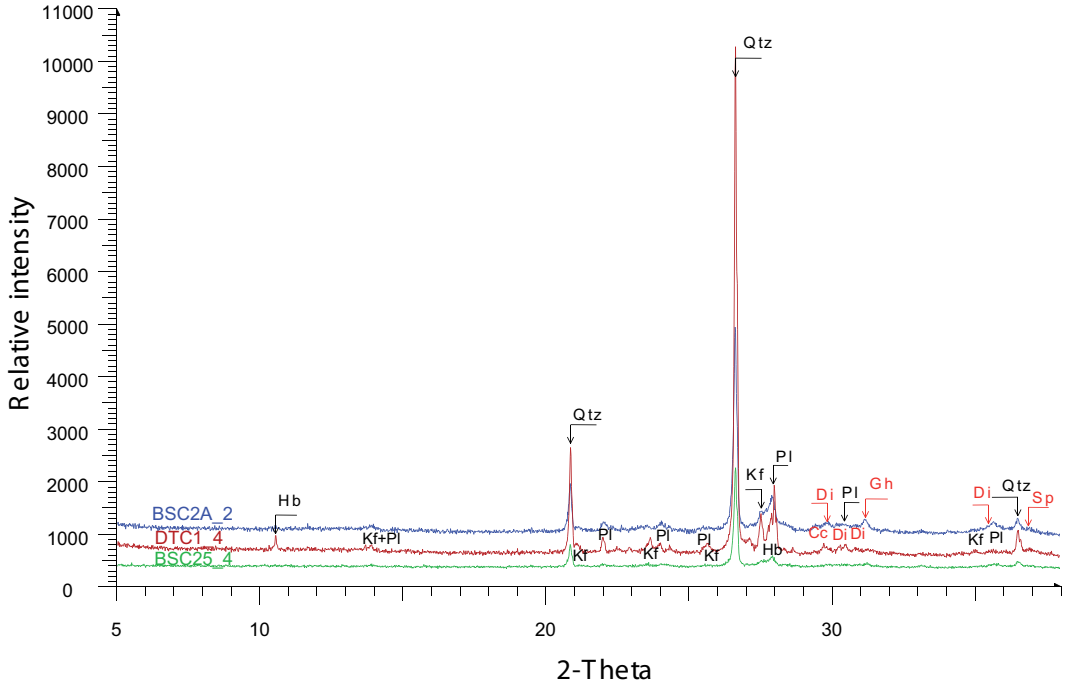

FIGURE 2.27 – *Diagrammes de diffraction des rayons X sur poudre pour trois échantillons de céramique (Grèce, datés du néolithique). Abréviation ; Qtz : Quartz, Pl=plagioclase (albite ou bytownite), Kf= feldspath-K (orthoclase), Di=diopside, Gh= gehlenite, Hb=hornblende, Tr= tremolite, Ep=epidote, Cc= calcite, Mi= mica blanc (illite ou muscovite), Sm= smectite, Sp : spinelle.*

à un état énergétique de base, il peut être absorbé par un nucléus du même isotope, ce dernier passant alors à son tour à un état excité. La source de rayonnement communément utilisée en spectroscopie Mössbauer est le ^{57}Co, qui se désintègre en ^{57}Fe par capture d'électron avec un temps de demi-vie de 270 jours. Le ^{57}Fe engendré par cette désintégration libère une énergie de 14.4 keV lors de son passage à l'état de repos. Ce rayonnement émis excite les atomes ^{57}Fe de l'échantillon absorbeur. Les échantillons naturels ne contiennent que 2% de cet isotope environ, mais cela se révèle suffisant pour obtenir de bons spectres. Une partie de l'énergie peut être en partie perdue dans la matrice par vibrations (phonons) pendant l'émission ou l'absorption de rayon γ. La résonance Mössbauer dans la matière absorbante peut être "décalée" ou "éclatée" par les interactions (dites hyperfines) entre les nuclei et leur environnement solide. Ce sont ces paramètres qui fournissent des informations quant à l'état physique et chimique du Fer. Pour explorer le spectre hyperfin de l'échantillon, l'énergie des rayons γ balaie une gamme de fréquences par effet Doppler. Ainsi, la source est mobile et se déplace à quelques mm/s. Les interactions hyperfines sont de trois types (Fig. 2.28 :

– **Le déplacement isomérique (IS Isoméric Shift)** : il provient d'une différence d'environnement chimique entre la source et l'absorbeur, ceci modifiant légèrement

le puits d'énergie potentiel entre les deux. Ce phénomène provoque le déplacement du spectre sur l'échelle de vitesse (Fig. 2.28). Les mesures de décalage sont relatives au ^{57}Fe dans une matrice de fer métal. Si l'absorbeur contient des ions Fe^{3+}, le déplacement isomérique est de 0.4 mm/s alors que s'il contient des ions Fe^{2+} de déplacement est de l'ordre de 1.4 mm/s. La règle générale est la suivante : plus les liaisons sont covalentes, et moins le décalage isomérique est important. Par exemple, le fer en configuration tetrahédrique (Fe^{3+}) est plus covalents que le fer en configuration octaédrique (Fe^{2+}), ce qui explique la différence de décalage isomériques pour les ions ferreux et ferriques. Ceci permet de déterminer sans ambiguïté l'état d'oxydation du fer.

– **L'éclatement quadripolaire (EQ Electric quadrupole interaction)** : il intervient pour des atomes de ^{57}Fe dans un environnement de faible symétrie électronique. Il en résulte une interaction entre le moment quadripolaire nucléaire et le gradient de champ électrique du noyau. Ce type d'interaction affecte seulement l'état excité et divise le niveau énergétique en sous-niveaux en paire mais n'affecte par le centre du spectre (Fig. 2.28). De manière général, les ions Fe^{3+} ont de faibles gradients électriques, correspondant à de faibles interactions quadripolaires ($\approx$ 0.7 mm/s) alors que les ions Fe^{2+} ont des gradients électriques relativement forts, à l'origine de fortes interactions quadripolaires ($\approx$ 3.0 mm/s).

– **L'interaction magnétique hyperfine (Magnetic hyperfine interaction)** : ce phénomène se produit par interaction entre le moment magnétique dipolaire et le champ magnétique des électrons du ^{57}Fe. Ceci conduit à l'effet Zeeman et à la formation de sous niveaux énergétiques pour l'état de base et l'état excité (Fig. 2.28). Cet effet ne se produit que dans des solides magnétiquement ordonnés (ferro-, ferri- et antiferromagnétiques). Dans les matériaux paramagnétiques, les spins magnétiques des ions changent d'orientation tellement rapidement que le noyau ne ressent uniquement qu'une moyenne nulle.

La spectroscopie Mössbauer est utilisée pour distinguer des minéralogies qui sont difficiles à déterminer avec les techniques plus traditionnelles. La détermination d'un mélange magnétite-maghémite en est un bon exemple. Alors que la magnétite est facilement identifiable par son point de Curie ou sa transition de Verwey, la maghémite l'est plus difficilement. La signature spectrale dépend de la proportion entre les différents minéraux et permet donc de les distinguer. La détermination de grains ultra-fins super-paramagnétiques sont souvent difficiles à identifier également. La température de déblocage ainsi que la dépendance de fréquence peuvent donner une information sur leur présence mais guère plus. La spectroscopie Mössbauer à température ambiante et à basse température (Azote ou Hélium liquide) permet d'obtenir des spectres caracté-

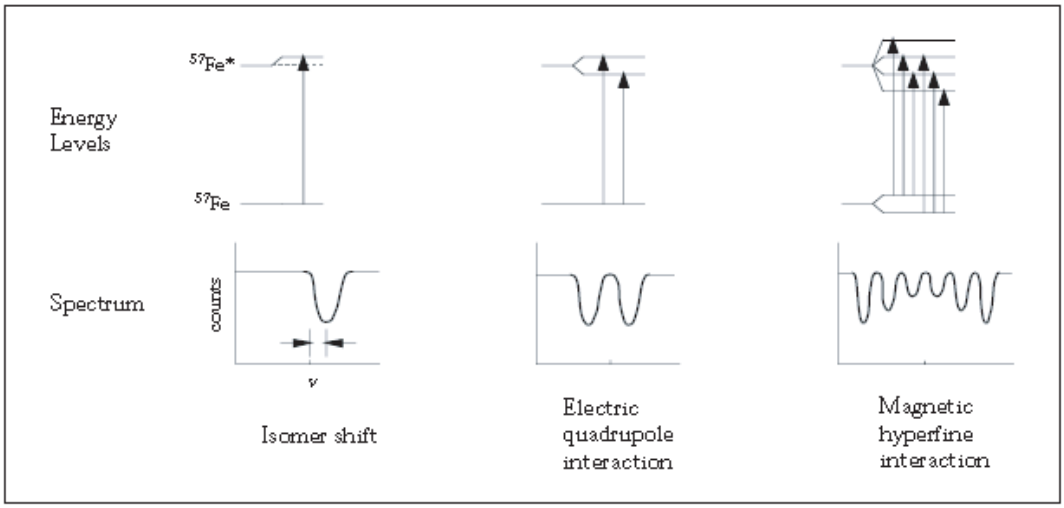

FIGURE 2.28 – *Diagrammes d'énergie et spectres associés pour les trois principales interactions. Un échantillon donnée peut possédé un spectre résultant de la superposition d'une combinaison de ces trois spectres.*

ristiques (Roggwiller and Kundig, 1973; Rivas-Sanchez et al., 2009) et ainsi d'identifier facilement des grains superparamagnétique.

Application à l'archéomagnétisme La spectroscopie Mössbauer peut également être utilisée en archéologie (Creagh and Bradley, 2000). En effet, la cuisson des poteries entraîne une modification physique et chimique de la fraction argileuse et de la fraction d'oxydes et oxy-hydroxydes de fer. Les argiles contiennent toutes du Fer en proportion plus ou moins variable (1 à 10 % en masse). Le spectre Mössbauer dépend donc des argiles initiales mais également de la manière avec laquelle elles sont cuites. Dans les fours, la cuisson peut être réalisée sous différentes conditions : milieu oxydant, réduit ou changeant. La température de cuisson et le temps de refroidissement sont également des paramètres importants du processus de fabrication. Dans quelle mesure peut-on tirer des conclusions quant à l'étude du spectre Mössbauer des poteries ? Plusieurs expériences ont été réalisées dans des répliques de fours anciens ou dans des fours excavés, mais pour lesquels les contrôles sont difficiles. Les expériences de chauffe en laboratoires présentent une part importante des études sur le sujet. Il est cruciale de pouvoir contrôler parfaitement l'atmosphère, la température de chauffe ainsi que la vitesse de refroidissement (Wagner et al., 1998a). Il en résulte que pour des températures de 500°C environ, l'équilibre thermodynamique est atteint pour 2h de chauffe, alors que pour des températures plus faibles, les réactions sont plus lentes et le temps de chauffe peut jouer de manière importante sur l'état du fer dans le matériau chauffé. Une autre question concerne le temps mis pour que la température à l'intérieur et à l'extérieur de la céramique soit identique. L'étude de la conduction thermique dans les céramiques a

montré que l'équilibre thermique est atteint en 5 minutes environ pour une épaisseur de l'ordre du centimètre (Wagner et al., 1998a). Mais l'information principale pouvant être obtenue à partir d'un spectre Mössbauer est la température de cuisson. Pour cela, il faut supposer que le matériau n'a pas été cuit en milieu réduit puis oxydé mais cuit en milieu oxydant (Creagh and Bradley, 2000). Lors de la cuisson en milieu oxydant, les paramètres du spectre Mössbauer à température ambiante les plus sensibles durant la cuisson sont le QS de l'ion trivalent Q_{Fe3+} et la fraction non magnétique A_{nm} (fraction de tous les éléments qui ne présentent pas d'interactions magnétiques) (Wagner et al., 1998b; Murad and Wagner, 1998; Wagner et al., 1998a). Q-Fe^{3+} montre une augmenta-

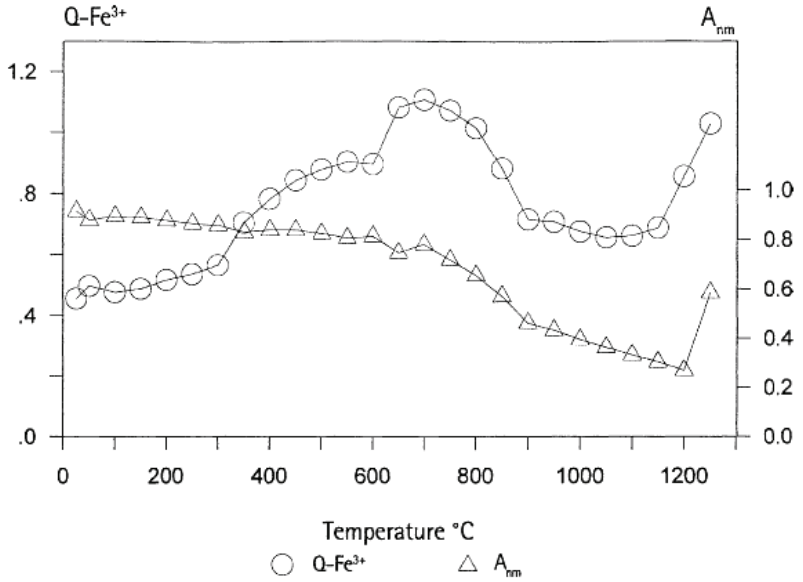

FIGURE 2.29 – *Dépendance de certains paramètres Mössbauer à température ambiante en fonction de la température de cuisson de l'argile Batán Grande. Q-Fe^{3+} (cercles) est la éclatement moyen quadripolaire du Fe^{3+} et A_{nm} (triangles) est la fraction du fer non magnétique (Fe^{2+} et Fe^{3+}) (d'après Murad and Wagner (1998)).*

tion caractéristique durant la cuisson entre 400 et 700°C alors qu'il décroit à partir de 800°C. A_{nm} décroit lorsque les oxy-hydroxides sont convertis en hématite entre 200 et 400°C et entre 800 et 900°C lorsque les ions fer structuraux sont libérés et deviennent de l'hématite (Fig. 2.29). La combinaison de ses deux paramètres peut donc permettre d'obtenir une bonne idée de la température de cuisson de la poterie.